physica status solidi b

phys. stat. sol. (b) **244**, No. 1, 474–479 (2007) / **DOI** 10.1002/pssb.200672581

Coulomb crystal and quantum melting in electron–hole plasmas of semiconductors under high pressure

Vladimir Filinov[*, 1, 2], **Michael Bonitz**[2], **Vladimir Fortov**[1], **Holger Fehske**[3], and **Pavel Levashov**[1]

[1] Institute for High Energy Density RAS, Izhorskay 13/19, Moscow 125412, Russia
[2] Christian-Albrechts-Universität zu Kiel, Institut für Theoretische Physik und Astrophysik, Lehrstuhl Statistische Physik, Leibnizstraße 15, 24098 Kiel, Germany
[3] Institut für Physik, Ernst-Moritz-Arndt-Universität Greifswald, Domstraße 10a, 17489 Greifswald, Germany

Received 16 June 2006, accepted 14 August 2006
Published online 12 December 2006

PACS 62.50.+p, 71.15.–m, 71.35.Ee

A phase diagram for variable hole to electron mass ratio of two-component Coulomb crystals is presented as result of the first-principle computer simulations. A critical mass ratio for the existence of quantum Coulomb crystals is of the order of 80 in three dimensions. At very low temperature the electron–hole system with decreasing hole mass can form antiferromagnetic crystal structure composed by two perfect hole lattices each consisting of the holes with the same spin projections.

1 Introduction

The present paper applies the quantum path integral Monte Carlo method (PIMC) to electron–hole plasmas (two-component plasma, TCP) with strong mass-asymmetry. In contrast to hydrogen (and similar) plasmas, here also the heavy component (the holes) has to be treated quantum mechanically [1, 2]. Section 2 gives the brief theoretical background. Then an extensive numerical study of a two-component Coulomb systems is presented in Section 3. In particular the electron–hole configurations, spin-dependent and spin-averaged pair distribution functions and the electron–hole phase diagram for variable hole to electron mass ratio are calculated in a wide range of temperatures and densities.

2 Path integral representation of thermodynamic quantities

We consider a neutral two-component plasma consisting of $N_e = N_h = N$ electrons and holes in equilibrium with the Hamiltonian $\hat{H} = \hat{K} + \hat{U}^c$, containing kinetic energy $\hat{K}$ and Coulomb interaction energy $\hat{U}^c = \hat{U}^c_{hh} + \hat{U}^c_{ee} + \hat{U}^c_{eh}$ contributions. The thermodynamic properties in the canoncial ensemble with given temperature T and fixed volume V are fully described by the density operator $\hat{\rho} = e^{-\beta\hat{H}}/Z$ with the partition function

$$Z(N_e, N_h, V; \beta) = \frac{1}{N_e! N_h!} \sum_{\sigma} \int_V dq\, \rho(q, \sigma; \beta)\,, \tag{1}$$

[*] Corresponding author: e-mail: filinov@ok.ru, Phone: +007 495 931 07 19, Fax: +007 495 485 79 90

where $\beta = 1/k_B T$, and $\rho(q, \sigma; \beta)$ denotes the diagonal matrix elements of the density operator at a given value σ of the spin variable. In Eq. (1), $q = \{q_e, q_h\}$ and $\sigma = \{\sigma_e, \sigma_h\}$ are the spatial coordinates and spin degrees of freedom of the electrons and holes, i.e. $q_a = \{q_{1,a} \dots q_{l,a} \dots q_{N_a,a}\}$ and $\sigma_a = \{\sigma_{1,a} \dots \sigma_{l,a} \dots \sigma_{N_a,a}\}$, with $a = e, p$.

Of course, the exact density matrix of interacting quantum systems is not known (particularly for low temperatures and high densities), but it can be constructed using a path integral approach [3, 4] based on the operator identity $e^{-\beta \hat{H}} = e^{-\Delta\beta \hat{H}} \cdot e^{-\Delta\beta \hat{H}} \dots e^{-\Delta\beta \hat{H}}$, where $\Delta\beta = \beta/(n+1)$, which allows us to rewrite the integral in Eq. (1)

$$\sum_{\sigma} \int dq^{(0)} \rho(q^{(0)}, \sigma; \beta) = \int dq^{(0)} \dots dq^{(n)} \rho^{(1)} \cdot \rho^{(2)} \dots \rho^{(n)} \times \sum_{\sigma} \sum_{P_e} \sum_{P_h} (\pm 1)^{\kappa_{P_e} + \kappa_{P_h}} \mathcal{S}(\sigma, \hat{P}_e \hat{P}_h \sigma'_a) \times \hat{P}_e \hat{P}_h \rho^{(n+1)}|_{q^{(n+1)} = q^{(0)}, \sigma' = \sigma} . \quad (2)$$

The spin gives rise to the spin part of the density matrix ($\mathcal{S}$) with exchange effects accounted for by the permutation operators $\hat{P}_e$ and $\hat{P}_h$ acting on the electron and hole coordinates $q^{(n+1)}$ and spin projections σ'. The sum is over all permutations with parity κ_{P_e} and κ_{P_h}. In Eq. (2) the index $k = 1 \dots n+1$ labels the off-diagonal high-temperature density matrices $\rho^{(k)} \equiv \rho\left(q^{(k-1)}, q^{(k)}; \Delta\beta\right) = \langle q^{(k-1)} | e^{-\Delta\beta \hat{H}} | q^{(k)} \rangle$. Accordingly each particle is represented by a set of $n+1$ coordinates ("beads"), i.e. the whole configuration of the particles is represented by a $3(N_e + N_h)(n+1)$-dimensional vector $\tilde{q} \equiv \{q_{1,e}^{(0)}, \dots q_{1,e}^{(n+1)}, q_{2,e}^{(0)} \dots q_{2,e}^{(n+1)}, \dots q_{N_e,e}^{(n+1)}; q_{1,h}^{(0)} \dots q_{N_h,h}^{(n+1)}\}$. For PIMC details see [5, 6].

3 Coulomb crystallization

For qualitative estimations of TCP crystal parameters let us consider well known results of one-component plasma (OCP). The necessary condition for the existence of a crystal in the OCP is that the mean hole Coulomb interaction energy, $e^2/\bar{r}$ ($\bar{r}$ denotes the mean inter-hole (or inter-electon) distance), exceeds the mean kinetic energy (thermal energy $3/2 k_B T$ or Fermi energy E_F in classical or quantum plasmas, respectively) by a factor Γ larger than Γ^{cr} which, in a classical OCP is given by 175 (137) in 3d (2d) [7, 8]. So for the existence of a Coulomb crystal in the presence of a classical uniform gas of electrons, we first require that the heavy component is able to form a classical OCP crystal, i.e. $\Gamma \geq \Gamma^{cr}$ and, secondly, that the electrons do not destroy that crystal, e.g., as a result of screening of the heavy particle interaction.

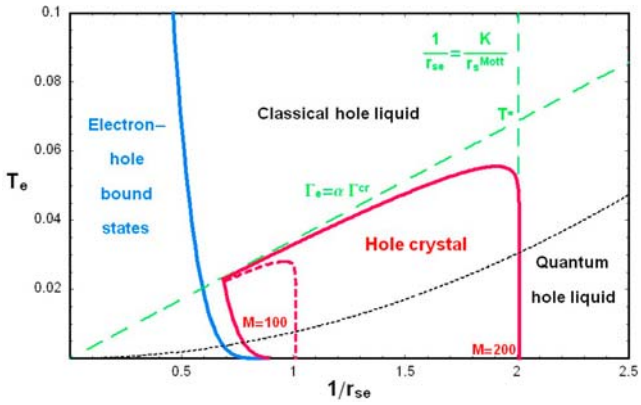

Fig. 1 (online colour at: www.pss-b.com) Qualitative phase diagram of a two-component plasma in the plane of dimensionless electron temperature $T_e = 3k_B T/2E_B$ and density parameter $1/r_{se}$. The blue line indicates the boundary of the Coulomb bound state phase given by $r_s^{Mott}(T_e)$. The red full (dashed) line is the boundary of the hole crystal for $M = 200$ ($M = 100$) with the asymptotics given by $\Gamma \geq \Gamma^{cr}$ (green dashed lines) [2].

However, the main obstacle for the crystal turns out to be the formation of bound states (atoms, excitons with binding energy E_B and etc.), because this reduces the h–h correlation energy causing violation of condition $\Gamma \geq \Gamma^{cr}$. Therefore, we require that no significant fraction of heavy particles is trapped in Coulomb bound states. This crystal of heavy particles will survive in the presence of electrons only if bound states are unstable, which, occurs due to pressure ionization at high densities above the Mott density, i.e. $r_{se} \equiv \overline{r}/a_B \leq r_s^{Mott} \approx 1-2$ (a_B denotes the effective Bohr radius). In a quantum OCP at zero temperature the coupling strength is measured by the Brueckner parameter, $r_{se} \equiv \overline{r}/a_B$, with a critical value for crystallization of $r_s^{cr} \approx 33$ (100) in 2d (3d) [9, 10]. The condition for crystallization of the holes follows from the quantum OCP result, $r_{se} = \overline{r}/a_B \geq r_s^{cr}$.

Now let us discuss the qualitative phase diagram of the TCP. Consider first the case of a hole crystal in semiconductors which is embedded into dense Fermi gas of electrons, see Fig. 1. The holes behave classically above the black dotted line and quantum-mechanically below (this line is given by $n_h \Lambda_h^3 = 1$, where $\Lambda_h = h/\sqrt{2\pi m_h k_B T_h}$ is the hole deBroglie wave length). The e–h bound state phase is shown in the left part and contains excitons and biexcitons. On leaving this phase across its boundary (given by the blue line $r_{se}(T_e) = r_s^{Mott}(T_e)$) the fraction of bound states rapidly vanishes in favor of unbound e–h pairs with the holes showing liquid-like behavior. Upon further compression (at low temperatures $T_e < T^*$ related to condition $\Gamma > \Gamma^{cr}$) the hole liquid crystallizes, provided the hole are classical particles with large enough mass (above the black dotted line). At the density $1/r_{se} = 2$ quantum melting of the crystal is observed at zero temperature (vertical dashed green line). The entire hole Coulomb crystal phase for $M = 200$ is marked by the full red line in Fig. 1. When M is reduced the crystal phase shrinks (see the red dashed line corresponding to $M = 100$) until for $M = M^{cr}$ it vanishes.

Coulomb crystallization of the holes and quantum melting were directly verified by the PIMC simulation. Presented in Fig. 2 snapshots show of the electron–hole states in the simulation box at fixed temperature and density, but for decreasing values of $M = m_h/m_e$. In all figure parts, the electrons form a nearly homogeneous Fermi gas – the individual electrons penetrate each other and extend far beyond the main simulation cell shown by the grid lines (to simulate a macroscopic system, this cell is periodically repeated in three (X, Y, Z) space directions). At the same time, the hole arrangement changes dramatically. At $M = 800$ holes are periodically ordered in space, at $M = 100$ and between $M = 100$ and 50 the holes crystal melts, at $M = 50$ the hole structure resembles liquid and at $M = 1$, the holes are in a gas-like state (similar to the electrons). The figure also clearly shows the mechanism of this quantum phase transition: with increase of M the individual hole wave packets shrink continuously until at $M = 800$ they collapse into a dot. The crystal melts when the decay length of the hole wave functions exceeds a critical size.

The quantum crystal–liquid transition at fixed temperature and density ($r_{se} = 0.63$) is further supported by the behavior of the spin-averaged and spin-dependent pair distribution functions (PDFs), shown in Fig. 3a)–d). The PDF g_{hh} demonstrate a hole crystal formation with increasing hole mass. At the mass ratios, density and temperature, when the hole ordering exists, the holes are still well localized, while the electrons are strongly degenerate and delocalized (see Fig. 2). In our simulation we can not

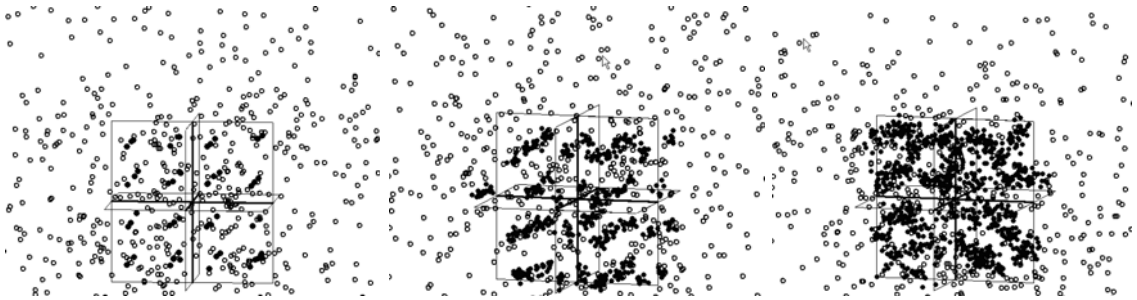

Fig. 2 Electron–hole snapshots for $k_B T/E_b = 0.064$, $r_{se} = 0.63$, $M = 800, 100, 50$ (from left to right, respectively). Empty (filled) circles are electron (hole) beads.

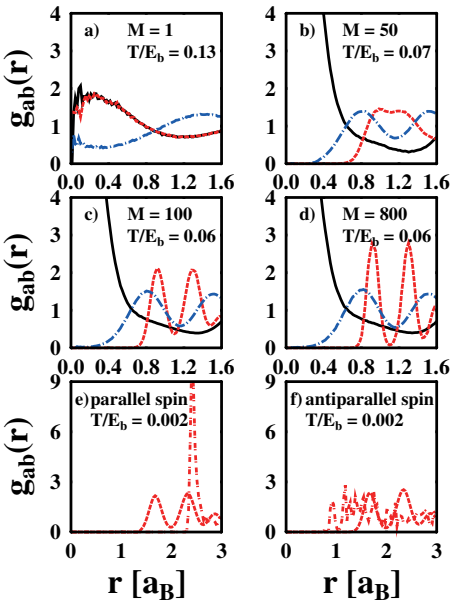

Fig. 3 (online colour at: www.pss-b.com) For quantum liquid – crystal hole transition at $r_{se} = 0.63$ the PDF g_{ab} averaged over spin projections are shown on figures a), b), c) and d). Solid lines present g_{ee}, dashed lines – g_{hh}, dotted-dashed lines – g_{eh}. The PDF g_{hh} for parallel e) and antiparallel f) spin projections are related to the transition of the hole crystal ($M = 400$ – dashed lines) to the antiferromagnetic crystal structure ($M = 100$ – dotted-dashed lines) with decreasing hole mass at $r_{se} = 1.13$.

resolve the energy spectrum but observe a thermal averages of all allowed energies. At the same time the simulations yield information about the spatial distribution of the all particles. As the PDFs g_{eh} and g_{ee} show, we observe a inhomogeneous space distribution of electrons. The physical evidence of this phenomenon can be understood from the behavior of g_{ee} and g_{eh} (Fig. 3b)–d)) and electron–hole snapshots on Fig. 4. Functions g_{ee} for ordered hole structures have the sharp peaks at small distances between electrons, while g_{eh} are periodically oscillating functions. Peak of g_{ee} exists only if the holes are ordered. So the density of the highly degenerated nearly free electrons in a hole periodic and quasi-periodic potential field is nonuniform and has interference maxima (see Fig. 4) related to the variation of the modulus of the electron wave functions according to the Bloch theorem and electron energy band structure. Quasi-lattice of negative charges related to these maxima lowers the crystal energy. So this quasi-lattice increases the critical temperature and reduces the critical value of Γ^{cr} for hole crystallization. As consequence at finite temperature the crystal phase is more stable than predicted by the OCP plasma model in which the electrons are assumed to form a strictly uniform background. For mass ratios smaller than 50 and temperature $k_B T/E_B > 0.064$ the hole ordering is destroyedand this peak in electron–electron PDFs disappears. With decrease hole mass at some point the hole wave length becomes so large that the holes with nonzero probability can invade the space of their nearest neighbors and disturb them, so the melting process initiates at $M = 75 - 50$. This crystallization threshold value of M in three-dimensional plasmas in semiconductors also agree with results of [11] ($M \sim 80$). Such values are feasible e.g. in the intermediate valence system Tm [Se,Te] under pressure [12, 13]. PIMC calculations show also that quantum melting agrees with the Lindemann criterion.

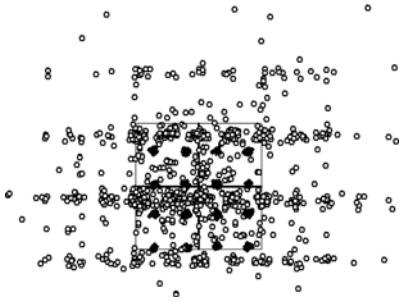

Fig. 4 Electron–hole snapshots for $k_B T/E_B = 0.002$, $r_{se} = 3$, $m_h = 800$, $m_e = 2.1$. Empty (filled) circles are electron (hole) beads.

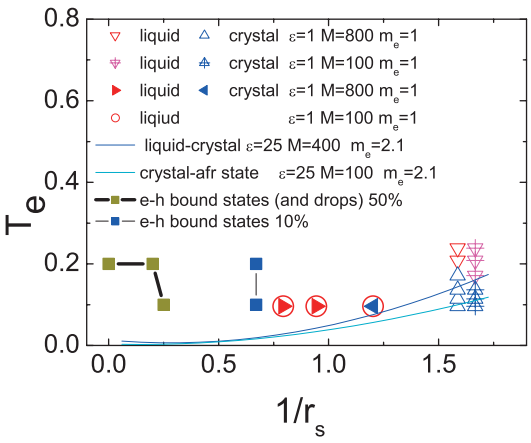

Fig. 5 (online colour at: www.pss-b.com) PIMC phase diagram of electron–hole plasma. The PIMC triangles directed downward (upward) and to the right (left) correspond to liquid (crystal) structure. The light-grey (red) color relates to the hole liquid phase, while the dark-grey (blue) one relates to the hole crystal.

Figure 3e) and f) demonstrate that at fixed density and very low temperature the electron–hole system with decreasing hole mass can form antiferromagnetic crystal-like structure composed by two perfect hole lattices each consisting of the holes with the same spin projections. The physical reason of this phenomenon is the strong Fermi repulsion between particles with the same spin projection. Correlation between lattices is defined only by an effective force repulsion, which is weaker at lower hole mass due to the tunneling of the holes.

Figure 5 presents electron–hole phase diagram obtained by PIMC. In the left lower corner, as in the Fig. 1, at low temperatures electrons and holes are in the bound states. This region is bounded by lines related to the 50% and 10% fraction of e–h bound states (estimations of the e–h bound states is given, for example, in [14]). With increasing density at fixed temperature (rightwards) bound states vanish and the Mott transition occurs. The dark-grey (blue) line shows the hole liquid-crystal transition, while the light-grey (green) line relates to transformation of the hole crystal to antiferromagnetic crystal structure. As example, the PIMC calculations are shown by the color triangles and circles. The light-grey (red) color relates to the hole liquid phase and the dark-grey (blue) one relates to hole crystal.

The electron–hole phases in Fig. 5 qualitatively agree with estimations of the phase diagram (Fig. 1) based on the data known for one-component plasma. The main temperature distinction of the lines related to the liquid-crystal transition on Figs. 1 and 5 (by factor of order 1.5 – 2) is connected with higher stability of the TCP crystal discussed above. Periodic oscillations of electron density lowers the total energy and the hole crystal can exist at higher temperature than in OCP with fixed homogeneous negative background. The second difference of the phase diagrams is related to transition of hole crystal to the antiferromagnetic crystal structure.

Acknowledgements The work is done under financial support of RF President Grant No. MK-3993.2005.8 and of the RAS program No. 14 (Section 2) “Fundamental problems of information science and technology”. This work has been also partially supported by Award No. RUX0-000013-PZ-06 and No. Y2-P-11-02 of the U.S. CRDF for the Independent States of the Former Soviet Union and of Ministry of Education and Science of Russian Federation.

References

[1] M. Bonitz, V. S. Filinov, V. E. Fortov, P. R. Levashov, and H. Fehske, J. Phys. A, Math. Gen. **39**, 4717 (2006).
[2] M. Bonitz, V. S. Filinov, V. E. Fortov, P. R. Levashov, and H. Fehske, Phys. Rev. Lett. **95**, 235006 (2005).
[3] R. P. Feynman and A. R. Hibbs, Quantum mechanics and path integrals (McGraw-Hill, New York, 1965).
[4] V. M. Zamalin, G. E. Norman, and V. S. Filinov, The Monte Carlo Method in Statistical Thermodynamics (Nauka, Moscow, 1977), in Russian.
[5] V. S. Filinov, M. Bonitz, W. Ebeling, and V. E. Fortov, Plasma Phys. Control. Fusion **43**, 743 (2001).
[6] V. S. Filinov, High Temp. **13**, 1065 (1975); **14**, 225 (1976).
[7] C. C. Grimes and G. Adams, Phys. Rev. Lett. **42**, 795 (1979).

[8] H. DeWitt and W. Slattery, Contrib. Plasma Phys. **39**, 1 (1999).
[9] A. V. Filinov, M. Bonitz, and Yu. E. Lozovik, Phys. Rev. Lett. **86**, 3851 (2001).
[10] D. M. Ceperley and B. J. Alder, Phys. Rev. Lett. **45**, 566 (1980).
[11] A. A. Abrikosov, J. Less-Common Met. **62**, 451 (1978).
[12] B. Bucher, P. Steiner, and P. Wachter, Phys. Rev. Lett. **67**, 2717 (1991).
P. Wachter, B. Bucher, and J. Malar, Phys. Rev. B **69**, 0945021 (2004).
[13] B. I. Halperin and T. M. Rice, Rev. Mod. Phys. **40**, 755 (1968).
[14] H. Fehske, V. S. Filinov, M. Bonitz, V. E. Fortov, and P. R. Levashov, J. Phys. Conf. Ser. **11**, 139 (2005).